Micrometer-Scaled Gradient Surfaces Generated Using Contact Printing of Octadecyltrichlorosilane

Sung-Hwan Choi and Bi-min Zhang Newby*

Department of Chemical Engineering, The University of Akron, Akron, Ohio 44325-3906

Received June 11, 2003

Gradient surfaces are widely employed in biological studies for protein adsorption and cell attachment and growth. They also offer great potential in the areas of fluid flow and combinatorial experimental design for obtaining material properties and behaviors. Gradient surfaces are created with organosilanes by using the diffusion techniques proposed by Ewling and modified by Chaudhury. However, these techniques have limitations. They either generate a significant amount of organic waste or require well-controlled deposition conditions. In this paper, we propose a fast, convenient, reproducible, and inexpensive method that generates gradient surfaces with minimum waste generation. Particularly, we have adopted Whitesides's contact-printing technique to achieve a gradient by gradually varying the contact time over the contacted area using octadecyltrichlorosilane. Elastomeric stamps with different geometries and various radii of curvature are used to generate gradient surfaces at both millimeter and micrometer scales. With this approach, we are able to generate micrometer-scaled gradient surfaces with a gradient steepness 1−3 orders of magnitude higher than those generated using diffusion-based techniques. The energy gradient on these surfaces is verified by the dewetting of polymer (e.g., polystyrene) thin films and by the movement of picoliter and nanoliter water droplets on the surface devoid of other driving forces such as gravity, temperature gradients, or a pressure drop.

Introduction

Over the past few years, generating gradient surfaces with controllable nonuniform surface compositions has attracted much attention for investigating the behavior of molecules or supermolecules. In biological studies, energy gradient surfaces have been utilized to investigate the subtle changes in interactions between proteins and surfaces, the continuous effects of surface wettability on protein adsorption/desorption behavior, and the kinetics of the adsorption/desorption process.[1−3] Such surfaces have also been employed to determine the surface conditions for cell attachment and growth, proliferation, and phenotype changes.[4−7] The insight from these studies is then applied in the development of medical devices and artificial organs, along with bone and tissue replacements. In addition, gradient surfaces have been used as model substrates to build chemical architectures that contain particle density gradients, which can further be utilized for optical- or electronic-device development.[8,9] Other potential applications for gradient surfaces include driving fluid flow in microfluidic devices,[10] increasing heat-transfer efficiencies[11] in heating/cooling systems, and transporting fluid under microgravitational environments. An interesting experimental area for adopting gradient surfaces is the combinatorial method,[12,13] in which an entire library of information on material behavior under different experimental parameters can be generated with minimal time and material.

In general, two classes of techniques have been used for generating gradient surfaces. The first set of techniques concentrates on removing the outer surface layer of a substrate in a gradient manner through a procedure such as UV radiation[13] or chemical etching.[12,14] These methods mainly apply to polymers, ceramics, or metals. Contrary to this approach, the second class focuses on the addition of a monolayer or a thin film, through controlled deposition, onto the substrate. Depositing a monolayer, which can modify the surface properties without altering the bulk material properties, appears more attractive. One technique to control the deposition of a self-assembled monolayer (SAM) of organosiloxanes to a substrate in a gradient manner is by diffusing the organosilane molecules in a solution[1,15] or in the vapor phase.[11,16] The scale of the gradient surface generated using the diffusion approach normally ranges from several millimeters to a few centimeters, and the gradient steepness is 1−10 N/m^2. For the vapor-phase-diffusion method, the deposition conditions need to be well controlled. Also, when the solution-diffusion technique is used, a significant amount of organic waste is generated.

Recently, contact printing, developed by Whitesides and co-workers, has been widely adopted as an alternative approach for generating SAMs.[17−19] In this technique, an

* Corresponding author. E-mail: bmznewby@uakron.edu.

(1) Elwing, H.; Welin, S.; Askendal, A.; Nilsson, U.; Lundstrom, I. *J. Colloid Interface Sci.* **1987**, *119*, 203−210.
(2) Spijker, H. T.; Bos, R.; van Oeveren, W.; de Vries, J.; Busscher, H. J. *Colloids Surf., B* **1999**, *15*, 89−97.
(3) Wahlgren, M.; Welin-Klintstroem, S.; Arnebrant, T.; Askendal, A.; Elwing, H. *Colloids Surf., B* **1995**, *4*, 23−31.
(4) Ruardy, T. G.; Moorlag, H. E.; Schakenraad, J. M.; van der Mei, H. C.; Busscher, H. J. *J. Colloid Interface Sci.* **1997**, *188*, 209−217.
(5) Ruardy, T. G.; Schakenraad, J. M.; van der Mei, H. C.; Busscher, H. J. *J. Biomed. Mater. Res.* **1995**, *29*, 1415−1423.
(6) Lee, J. H.; Lee, H. B. *J. Biomed. Mater. Res.* **1998**, *41*, 304−311.
(7) Lee, J. H.; Lee, S. J.; Khang, G.; Lee, H. B. *J. Colloid Interface Sci.* **2000**, *230*, 84−90.
(8) Plummer, S. T.; Bohn, P. W. *Langmuir* **2002**, *18*, 4142−4149.
(9) Bhat, R. R.; Fisher, D. A.; Genzer, J. *Langmuir* **2002**, *18*, 5640−5643.
(10) Grunze, M. *Science* **1999**, *283*, 41−42.
(11) Daniel, S.; Chaudhury, M. K.; Chen, J. C. *Science* **2001**, *291*, 633−636.
(12) Ashley, K. M.; Carson Meredith, J.; Amis, E.; Raghavan, D.; Karim, A. *Polymer* **2003**, *44*, 769−772.
(13) Roberson, S. V.; Fahey, A. J.; Sehgal, A.; Karim, A. *Appl. Surf. Sci.* **2002**, *200*, 150−164.
(14) Jeon, N. L.; Dertinger, S. K. W.; Chiu, D. T.; Choi, I. S.; Stroock, A. D.; Whitesides, G. M. *Langmuir* **2000**, *16*, 8311−8316.
(15) Elwing, H.; Welinklintstrom, S. *Bioprocess Technol.* **1996**, *23*, 257−272.
(16) Chaudhury, K.; Whitesides, G. M. *Science* **1992**, *256*, 1539−1541.

10.1021/la035027l CCC: $25.00
Published on Web 08/07/2003

elastomeric stamp and a dilute "ink" solution of octadecyltrichlorosilane (OTS) or thiols are employed. The structure and stability of an OTS monolayer generated with contact printing have been extensively studied by Jeon et al.[20] They observed that a closely packed OTS monolayer could be generated using an elastomer stamp and an ink of 10 mM OTS in hexane with only 30 s of contact on a cleaned and oxidized Si/SiO_X surface. Different surface coverages of OTS could be achieved by varying either the contact time or the ink concentration. On the basis of the results of Jeon et al., controlling the contact time enables the generation of an energy gradient surface by simply contact printing of OTS.

In this study, we report the generation of gradient surfaces by initiating minimum contact between the inked stamp and the surface (i.e., oxidized silicon wafer) and then gradually increasing the contact area while simultaneously decreasing the contact time from the initial contact region to the final contact region. An area with longer contact has more $-CH_3$-terminated OTS molecules deposited and, thus, a lower surface energy. The aim of this study was to generate various micrometer-scaled energy gradient surfaces by contact printing of OTS. The geometries of the gradient depend on the shapes of the elastomeric stamps that were fabricated from silicone Sylgard 184. The uncured elastomer was either placed inside suitable molds or shaped into the desired geometries on a fluorosiloxane-treated silicon wafer. Each of the stamps, with OTS as the ink, was separately brought into contact with a cleaned and oxidized silicon wafer, and the contact-printed area was gradually increased as the corresponding contact time decreased from initial contact to final contact. Our results show that well-defined gradient surfaces could be generated in a matter of seconds using the contact-printing technique. In addition, the size of the contact area could be controlled within tens to hundreds of micrometers. On these gradient surfaces, directional movements of picoliter or nanoliter water droplets were observed, suggesting it was possible to transport small quantities of fluids using such gradients. Quick drainage of the tiny droplets from the micrometer-scaled gradient surfaces was also noticed, indicating a possible application in heating/cooling or heat-exchanger systems to enhance the heat-transfer efficiency.[11]

Results and Discussion

Contact Printing of OTS with Various Contact Times. Before generating a gradient surface with contact printing, we verified the capability of generating different OTS surface coverages. Surfaces with varying surface energies were created by contact printing of a 2 mM OTS/hexane solution onto Si/SiO_X substrates using different contact times. Scanning probe microscopy (SPM) was utilized to evaluate the formation and surface coverage of OTS. Both topographic and lateral force images of contact-printed surfaces under several different contact times were obtained, and some of them are presented in Figure 1. The formation of OTS was indicated by the brighter (higher) domains in the topographic images and the corresponding darker (lower) domains in the lateral force images because the OTS monolayer has much lower friction than that of the Si/SiO_X substrate. After 1 s of contact time, OTS molecules were sparsely deposited throughout the contact area (Figure 1a). Then, after 10 s, disordered and loosely packed structures[21−23] began to assemble (Figure 1b), and after 20 s, closely packed but isolated, islandlike structures (Figure 1c) were formed. As these island domains grew in the lateral direction, secondary islands formed until finally, after 120 s, all the islands coalesced with each other to form a continuous layer.

The growth mechanism of the OTS monolayer contact-printed on the Si/SiO_X surface was speculated as the combination of the "island" model by Cohen et al.[24] and the "uniform" model by Wasserman et al.[25] Local evaluation at micrometer or nanometer scales indicated that the OTS molecules first formed islands consisting of disordered molecules and, as more molecules adsorbed onto the islands, the molecules extended fully by the increase of interchain van der Waals interactions. The monolayer was completed by the coalescence of these islands. The fully extended OTS monolayer was verified by the height (∼30 Å) of the primary islands, which was close to the chain length (∼26 Å)[26] of the OTS molecules. On the other hand, if relatively larger scales (hundreds of micrometers to millimeters) were evaluated, the monolayer formation appeared to be uniform with an increase in the thickness as the contact time increased. This was confirmed through thickness measurements with ellipsometry. The average monolayer thicknesses were 6, 9, 12, and 23 Å for contact times of 1, 10, 30, and 120 s, respectively.

Wettability, in terms of the contact angle measured on the contact-printed surface, was used as another means for characterizing the quality of the OTS monolayer formation. Both the advancing and receding contact angles of two probe liquids, water and methylene iodide, were measured using the sessile drop method, and the surface energy (γ_S, also presented in Figure 1) was estimated based on the contact-angle values.[27] The value of γ_S decreased rapidly from 1 s of contact (64 mJ/m^2) to 20 s of contact (46 mJ/m^2). It continued to decrease at a slower pace for the longer contact times, and reached a minimum of 26 mJ/m^2 at 120 s of contact. The surface-energy variation with contact time was further verified with contact mechanics (Johnson−Kendall−Roberts, JKR) studies. For the substrate contact-printed over 120 s, the work of the adhesion value measured with the JKR technique was 52 mJ/m^2, equating to a surface energy of ∼28 mJ/m^2. This surface energy was slightly higher than that of an ideally close-packed OTS monolayer (∼21 mJ/m^2),[28] suggesting that, even after 120 s of contact, occasionally uncovered SiO_X sites existed and the monolayer could be slightly disordered with the exposure of $-CH_2-$ (32 mJ/m^2)[29] of the OTS chains.

OTS Contact-Printed Gradient Surfaces. The above study proved that we could vary the OTS surface coverage,

(17) Xia, Y.; Whitesides, G. M. *Annu. Rev. Mater. Sci.* **1998**, *28*, 153−184.
(18) Xia, Y.; Whitesides, G. M. *Langmuir* **1997**, *13*, 2059−2067.
(19) Kumar, A.; Biebuyck, H. A.; Whitesides, G. M. *Langmuir* **1994**, *10*, 1498−1511.
(20) Jeon, N. L.; Finnie, K.; Branshaw, K.; Nuzzo, R. G. *Langmuir* **1997**, *13*, 3382−3391.
(21) Wasserman, S. R.; Tao, Y.-T.; Whitesides, G. M. *Langmuir* **1989**, *5*, 1074−1087.
(22) Tillman, N.; Ulman, A.; Schildkraut, J. S.; Penner, T. L. *J. Am. Chem. Soc.* **1988**, *110*, 6136−6144.
(23) Fadeev, A. Y.; McCarthy, T. J. *Langmuir* **2000**, *16*, 7268−7274.
(24) Cohen, S. R.; Naaman, R.; Sagiv, J. *J. Phys. Chem.* **1986**, *90*, 3054−3056.
(25) Wasserman, S. R.; Whitesides, G. M.; Tidswell, I. M.; Ocko, B. M.; Pershan, P. S.; Axe, J. D. *J. Am. Chem. Soc.* **1989**, *111*, 5852−5861.
(26) Bierbaum, K.; Grunze, M.; Baski, A. A.; Chi, L. F.; Schrepp, W.; Fuchs, H. *Langmuir* **1995**, *11*, 2143−2150.
(27) Good, R. J. *J. Adhes. Sci. Technol.* **1992**, *6*, 1269−1302.
(28) Chaudhury, M. K.; Whitesides, G. M. *Langmuir* **1991**, *7*, 1013−1025.
(29) Owens, D. K.; Wendt, R. C. *J. Appl. Polym. Sci.* **1969**, *13*, 1741−1747.

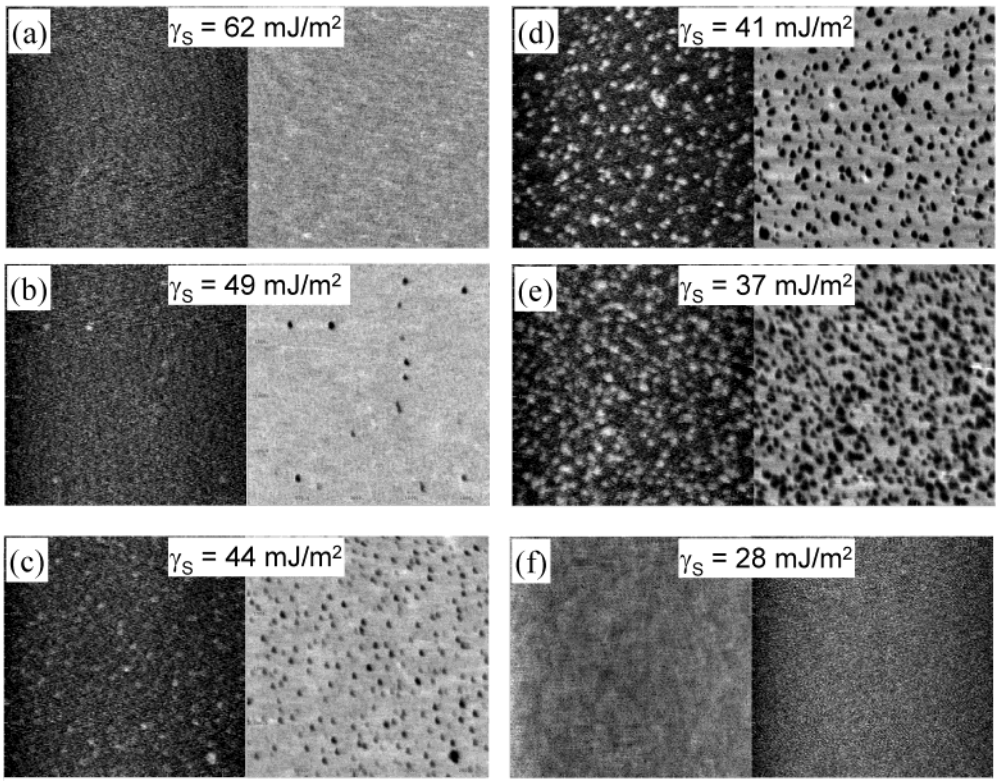

Figure 1. $2 \times 2\,\mu$m SPM topographic and lateral force images of contact-printed OTS on Si/SiO_x on the left and right, respectively, of each surface corresponding to a particular contact time. The higher regions in the topographic images correspond to the lower lateral force regions in the lateral force images, suggesting that these regions were covered with OTS molecules. The OTS domains grew with the contact time. With contact times of (a) 1 s, no visible islands were observed; (b) 10 s, small circular islands (~85 nm in diameter) were found; (c) 20 s, the number of the small islands was remarkably increased, and secondary islands were also observed among the primary islands; (d) 30 s, the islands grew in size and number; (e) 60 s, the density of the islands further increased, but the sizes became comparatively uniform; and (f) 120 s, the islands coalesced and started to form a continuous layer. The total surface energies, estimated using the two-liquid contact-angle method,[27] of each surface are also presented on the images. As the contact time increased, the surface energy of the OTS contact-printed area decreased.

thus generating surfaces with varying surface energies by contact printing. Furthermore, we showed that the surface coverage could be tuned by adjusting the length of the contact time and that an energy gradient could then be generated by gradually varying the contact time over the contact area during the contact printing of OTS onto a surface. Having this information, we wished to explore the effects of both scale and geometry on the energy gradient generated by the contact printing of OTS. A gradient scale mainly depends on the radius of curvature of the silicone stamp; therefore, stamps of various radii of curvature and geometries were fabricated, and the resulting gradient surfaces with sizes ranging from tens of micrometers to several millimeters were generated. The sketch in Figure 2 illustrates the generation of various gradient surfaces with the gradual and stepwise increase of the contact area or decrease of the contact time. The contact area as well as the contact time was controlled using a micromanipulator. Images in the right column of Figure 2 illustrate the energy gradient, indicated by the degree of gray scale, corresponding to the schematics in the left column. The area of initial stamping sustained the longest contact and, thus, the lowest γ_S (depicted as the darkest). The steepness of the gradient was achieved by controlling the rate of contact during the gradual contact or by using a combination of the contact increment and duration of contact during the stepwise contact. During the contact-printing experiment, we have noticed that when the stamp was very close to the substrate while approaching, it jumped into contact with the substrate and created a relatively large area of initial contact as compared to the gradient steps. This initial contact could reduce the effective gradient area of the total gradient surface. Also, we observed that the pressure applied on the stamp has minimum effects on the quality of the OTS monolayer generated.

For the gradient surfaces generated, we first attempted to characterize them by contact-angle measurements (inset of Figure 3). With relatively large (several millimeters) gradient surfaces, the overall gradient was clearly indicated by the asymmetric water drop having different contact angles at the opposite edges of the drop. However, even with millimeter-scaled gradient surfaces, it was difficult to use the contact angle to verify the detailed energy variation throughout the contact-printed area because of the insufficient resistance on the drop to temporarily maintain it in a particular location on the gradient surface for the measurement of the contact angle. By having insufficient resistive forces acting on the drop, as more water was added, the expansion of the three-phase contact line led to the instability of the drop on the surface because of the large unbalanced Young's force acting on it. Observations showed that the drop then moved toward the higher-energy region and began wetting outside the contact-printed region. In addition, other difficulties, such as pinning of the water drop at the low-energy region or severe distortion of the water drop, caused the measurement of the contact angle to be dubious. With micrometer-scaled gradient surfaces, the water drop used in the contact-angle measurement, normally having a base diameter in millimeters, either wetted the entire surface

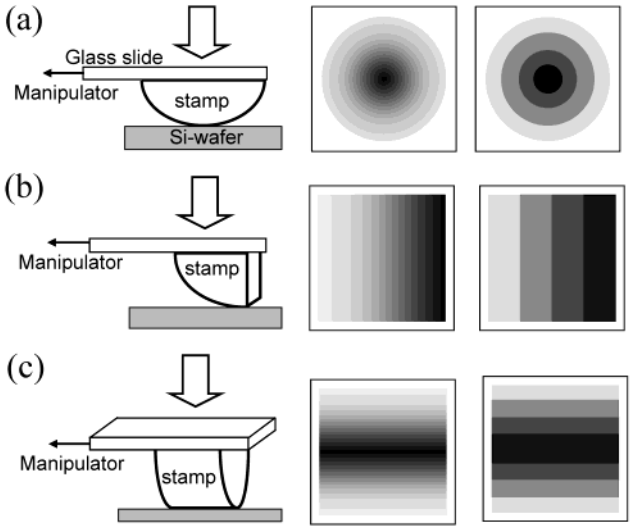

Figure 2. Schematic arrangements (left) for various gradient surfaces generated using contact printing of elastomeric stamps having different geometries. Radial (a), one-directional lateral (b), and symmetrical lateral (c) gradients were generated using hemispherical, quartercylindrical, and hemicylindrical stamps, respectively. The gradient was controlled by the contact duration, which was directly related to the surface energy. When a micromanipulator was used, a gradual (middle) or a stepwise (right) energy gradient could be generated by the gradual or stepwise increase of the contact area under increased compression. The darker areas indicate the more hydrophobic region where the contact time was longer. The sketch is not to scale.

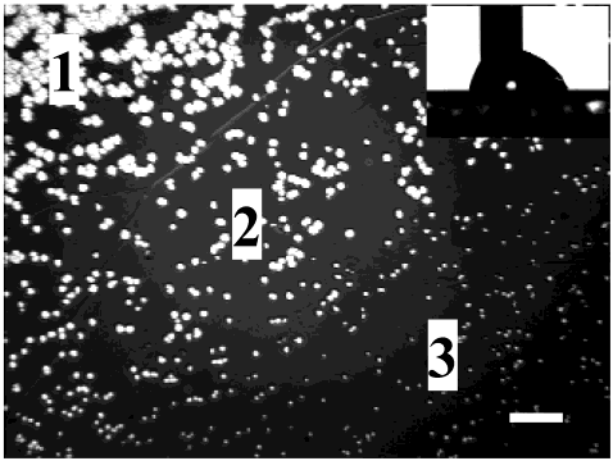

Figure 3. Optical microscopy image of a dewetted PS thin film on a radial gradient surface after the film had been annealed at 160 °C in air for 1 min. The gradient was generated by the gradual contact printing of OTS using a hemispherical stamp having a radius of curvature of ~20 mm. The image showed only a part of the total dewetted area on the gradient surface. Close to the center of the contact-printed region, most dewetted holes already coalesced. With an increased distance from the center (1 → 2 → 3), the dewetted hole size decreased, corresponding to the increased surface energy. The scale bar is 200 μm. The inset shows the shape of a water drop, with a base diameter of ~1.5 mm, placed somewhere between the center and the edge of the gradient surface. The needle needed to be immersed in the water drop to maintain the drop on a particular spot on the gradient surface; otherwise, the drop would move toward the higher-energy region and then wet outside (oxidized area not covered with OTS molecules) the contact-printed area. A difference of 22° in the advancing water contact angles from the two opposite edges of the drop was observed.

or was repelled from the contacted area and wetted its surroundings.

With contact-angle measurements not providing much useful information, we attempted to employ SPM for characterizing the gradient surfaces. However, we encountered difficulties in locating the exact regions of interest because OTS modified regions appeared to be identical to their surroundings to the naked eye or under an optical microscope without any additional visualization aids. Therefore, dewetting of a polymer thin film was utilized to visualize the geometry and steepness of the gradient surfaces and to qualitatively characterize our surfaces. According to our previous study,[30] as the surface energy decreased, the size of the dewetting hole at a particular annealing time or the rate of dewetting increased. Figure 3 represents an optical image that shows a portion of a dewetted polystyrene (PS) thin film on a radial gradient surface after the film had been annealed at 160 °C in air for 1 min.[31] The gradient was generated by gradual contact printing of OTS using a hemispherical stamp having a radius of curvature of ~20 mm. Most dewetted holes were observed to coalesce with each other close to the center of the contact-printed region, where the surface energy was the lowest. As the energy increased (from 1 to 3, as is shown in Figure 3), the dewetted hole size decreased.

Figure 4a–c represents the dewetting hole distributions on micrometer-scaled gradient surfaces corresponding to a radial, a one-directional lateral, and a bidirectional lateral gradient, respectively. The images were taken after the samples were annealed at 160 °C in air until discernible hole formation occurred. For these particular surfaces, the contact times were differentiated using stepwise contact to ensure the clarity of the gradient. In some cases, dewetted holes already coalesced at lower-energy regions, and as the surface energy increased, the decrease in the hole size from several tens of micrometers to less than 5 μm was noted. The stepwise or gradual variation of the dewetting hole size, thus, demonstrated an energy gradient corresponding to the different geometries on all the gradient surfaces, although borders were unclear in some cases due to the low density of the dewetting holes at each region corresponding to a particular surface energy. The same stamps were used in order to uniformly contact-print similar-sized areas with a contact time of 120 s, and the PS thin film dewetting studies were performed on these surfaces as comparisons to those on the gradient surfaces to address other factors that might contribute to the dewetting hole size distribution. The latter surfaces were defined as homogeneous surfaces, and the size of the dewetting holes was found to be uniform throughout the contact-printed regions in all the cases. A representative image is shown in Figure 4d.

Movement of Pico/Nanoliter Water Droplets on Gradient Surfaces. The movement of water droplets on micrometer-scaled gradient surfaces is an intriguing phenomenon that we wished to investigate further. Our droplets have a diameter of a hundred micrometers or less, and to our knowledge the movement of such small droplets caused solely by a surface-energy gradient has not been reported. An ultrasonic humidifier equipped with

(30) Choi, S.-H.; Zhang Newby, B.-m. *Langmuir* **2003**, *19*, 1419–1428.

(31) We have performed a degradation study of PS thin films of 800 Å annealed in air at 160 °C for different durations up to 1 h. The gel permeation chromatography results showed that even after 1 h of annealing, the molecular weight and molecular weight distribution varied only slightly from the unannealed sample. Therefore, only minimal thermal degradation should occur when our PS thin film was annealed in air at 160 °C, and the degradation would likely play a much smaller role in dewetting as compared to other factors, such as the substrate surface energy.

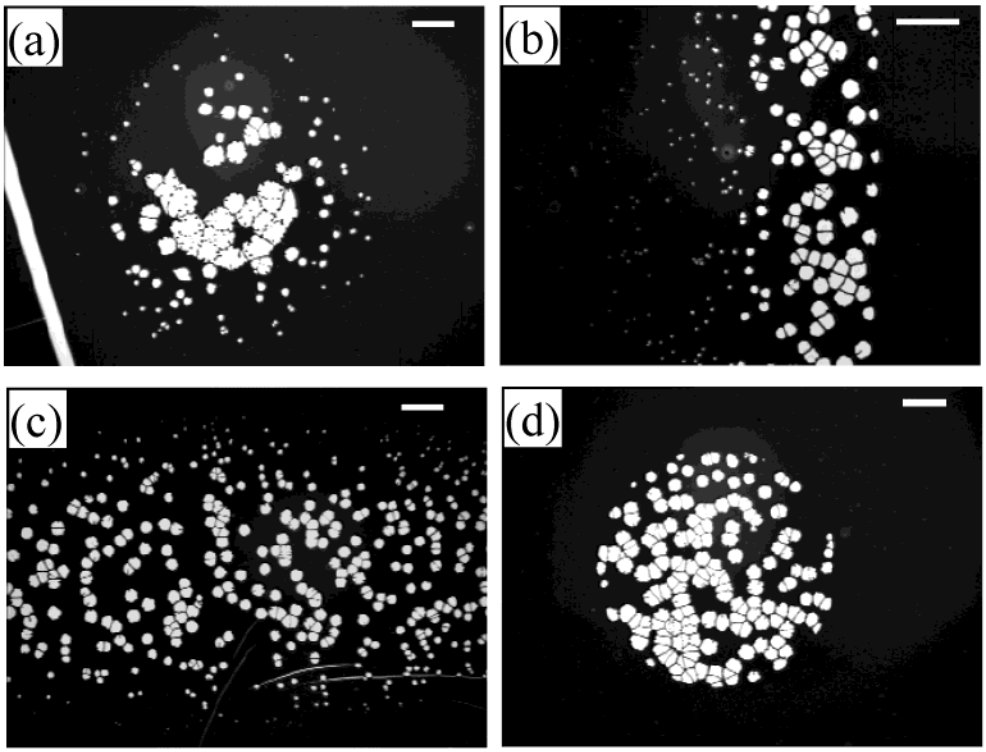

Figure 4. Optical microscopy images of dewetted PS thin films on a micrometer-scaled homogeneous surface and gradient surfaces with various geometries generated by contact printing of OTS. The radial gradient (a) and the one-directional lateral gradient (b) were generated by stepwise contact printing for 15 s for each step using a hemispherical stamp and a quartercylindrical stamp, respectively. The symmetrical lateral gradient (c) was generated by gradual contact printing for 30 s using a hemicylindrical stamp. The homogeneous surface (d) was generated by contact printing for 120 s using the same hemispherical stamp with a diameter of ~550 μm. While the dewetted hole size varied corresponding to the energy gradient on the gradient surfaces, a uniform dewetting hole size distribution was observed on the homogeneous surface. The annealing time, between 1 and 5 min, was varied from sample to sample to ensure that discernible dewetting holes could be observed on each surface. The scale bars are 100 μm.

a piezoelectric transducer was used to generate water droplets appropriate for the micrometer-scaled surface. The transducer produces ultrasonic frequencies that enable the generation and distribution of a cool water mist. The mist was guided toward the substrate by an air current that was also generated by the humidifier. The deposition of the water mist and behavior of the water droplets on the surface were monitored using an optical microscope video system. As the mist was deposited on the surface, tiny droplets, in the shape of spherical caps with a base diameter less than 5 μm, were formed. On the highly hydrophilic, noncontact-printed area, droplets quickly spread out to wet the surface and merged with each other to generate a thin water layer. Conversely, on the contact-printed area, the droplets continued to bead up, and as more mist was deposited, the droplets grew in size and occasionally merged with neighboring droplets.

Water-droplet movements on the homogeneous surface were found to differ substantially from those on the gradient surface (Figure 5), although both surfaces were generated using the same stamp and having a comparable total contact area. On the homogeneous surface, no directional movement of the water droplets was observed (Figure 5b). Instead, random movement activated by the coalescence among water droplets described by Daniel et al.[11] as the "two-dimensional random walk" was observed, and the center of mass was sustained.[32,33] With successive coalescences of water droplets and the addition of water from the mist, a large water drop finally formed near the center of the contact-printed area of the homogeneous surface.

In contrast to the homogeneous surface, on the gradient surface, directional movements corresponding to the direction of the energy gradient were observed at regions outside the initial contact (droplets 1−3 and 5 in Figure 5a). One result of such movements was that, during droplet coalescing, the center of mass of the merged droplets on the gradient surface was shifted in the direction of the gradient. This biased coalescence could induce directional hydrodynamic flow within the coalesced droplet. As the droplet size increased by merging, expectations were that the resulting unbalanced forces coupled with the internal flow would work to overcome the contact-angle hysteresis that hinders the droplet movements. In addition, water droplets (especially droplet 2 in Figure 5a) also grew by the addition of tiny water droplets from the mist; in this case, the three-phase contact line only expanded along the gradient toward higher-energy regions. This directional expansion of the three-phase contact line also assisted the directional coalescence along the gradient[11] and, thus, the movement of the water droplet.

To show that the droplet movement was driven primarily by an energy gradient, we considered other potential driving forces. One such force is the momentum carried by tiny droplets of the mist that occasionally deposited to the water droplet on the surface. The mass of each mist droplet was less than 0.1 ng, and its deposition velocity onto the surface was around 1 m/s, meaning the momentum of the mist droplet was on the order of 10^{-13} N·s. Such a small momentum, as was illustrated on the

(32) Zhao, H.; Beysens, D. *Langmuir* **1995**, *11*, 627−634.
(33) Andrieu, C.; Beysens, D. A.; Nikolayev, V. S.; Pomeau, Y. *J. Fluid Mech.* **2002**, *3453*, 427−438.

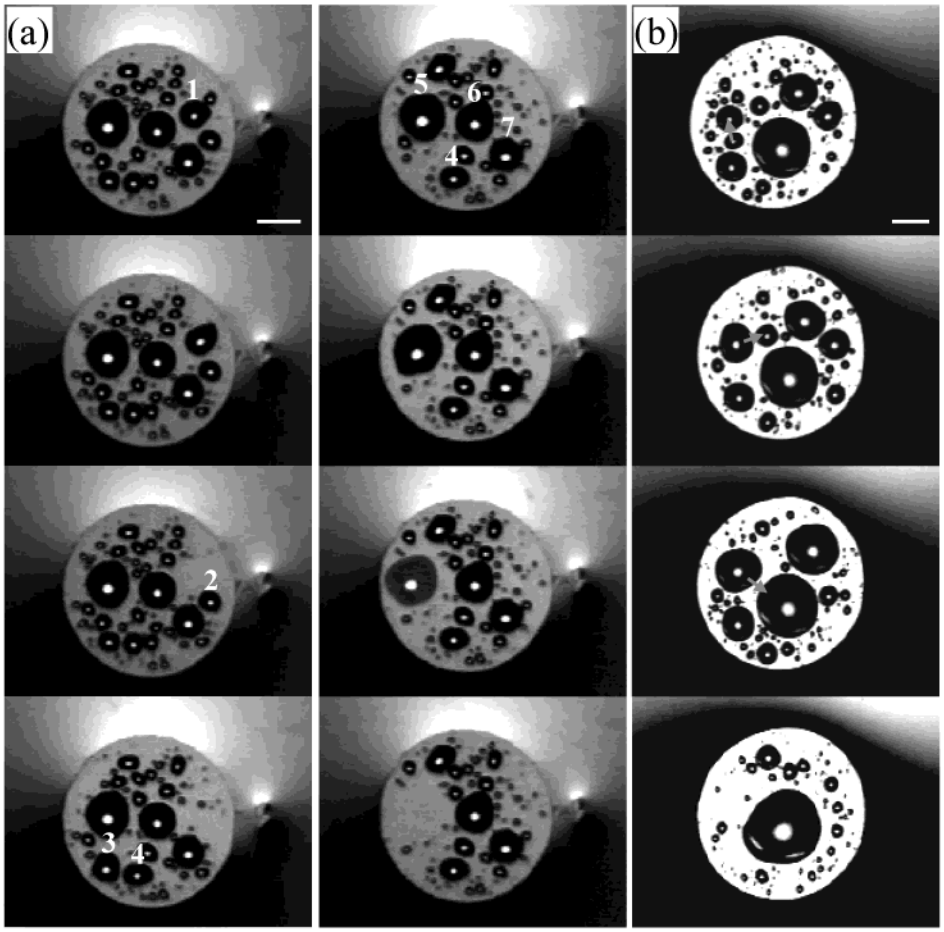

Figure 5. Behavior of water droplets on a radial gradient surface (a) compared to that on its corresponding homogeneous surface (b). The radial gradient surface (~400 μm across) was generated by the stepwise stamping of a hemispherical stamp having a radius of curvature of ~1 mm. The step increment was around 25 μm, and the time differentiation from one step to another was 5 s. On the gradient surface, the three-phase contact line of droplets 1 and 3−5 expanded while merging with neighboring droplets, and the center of the mass traveled along the direction of the energy gradient. For the particular droplet 5, it traveled around 30 μm with a velocity of ~150 μm/s along the direction of the gradient, quickly disappeared (~2 mm/s) when it was close to the edge of the gradient area, and then merged into the water layer surrounding the gradient surface. The subsequence images in part a were taken at 0, 0.23, 0.47, 2.9, 7.73, 7.77, 7.97, and 8 s. After merging, small droplet 4 (~50 × 70 μm elliptical-shaped base) was too far away from the edge (~50 μm away from edge) to be transported by the energy gradient, while droplet 6 (base diameter ~ 80 μm), located inside the initial contact region, experienced minimum or no driving force as a result of the flat energy gradient. At a later time (~7 s after the last frame in part a, not presented here), droplet 7 also merged with its neighboring droplets, moved along the gradient, and disappeared into the surrounding water layer. In contrast, on the homogeneous surface (~450 μm across), no directional but random movements of the droplet were observed. Directions of droplet movements are indicated by the gray arrows. The subsequent images in part b were taken at 0, 12, 31, and 61 s after the droplet started moving. The background outside the modified area was a continuous water film formed on the SiO_X surface. The scale bars in both sets of images are 100 μm.

homogeneous surface, could not initiate the motion of the water droplet as the mist was deposited. Because the sample surface was placed horizontally during the droplet movement experiment and no external driving forces were applied, other driving forces, such as gravitational force or pressure drop, were also ruled out.

The range of velocities we observed was in good agreement with the expected values that would result from the Marangoni effect[34] due to surface-energy variations. When well inside the gradient region but outside initial contact, droplets traveled at tens to hundreds of micrometers per second. When the droplets were very close (10−30 μm) to the edge of the gradient, the velocity increased to a few millimeters per second. For droplet 5 in Figure 5a, it traveled 30 μm in 0.2 s (150 μm/s) at first, and then it accelerated to ~1.8 mm/s when its leading edge was about 10 μm away from the border of the gradient surface and the water film. Because of this, we speculated that the energy gradient was much steeper near the edge as compared to the inner region of the gradient. When comparing the actual size of the contact-printed area with the apparent size of the nonwettable region, we noticed, in most cases, that the apparent area had a diameter of 10−30 μm greater than that of the actual contacted area. Two possible sources, as were indicated by Jeon et al.,[20] could lead to this result. One possibility is that the OTS molecules migrated on the surface from the edge of the contact region. Another possibility is that the OTS molecules diffused to the substrate from the part of stamp that was immediately adjacent to the contact-printed regions where only marginal separation between the stamp and the substrate existed during contact printing. The OTS coverage on this region could be very low. Although the region was nonwettable by water, the surface energy on this region could still be relatively high, resulting in a dramatic increase in unbalanced forces due to large surface-energy differences acting on the opposite edges of the droplet.

(34) Marangoni, C. G. M. *Ann. Phys. Chem. (Poggendorff)* **1871**, *143*, 337−354.

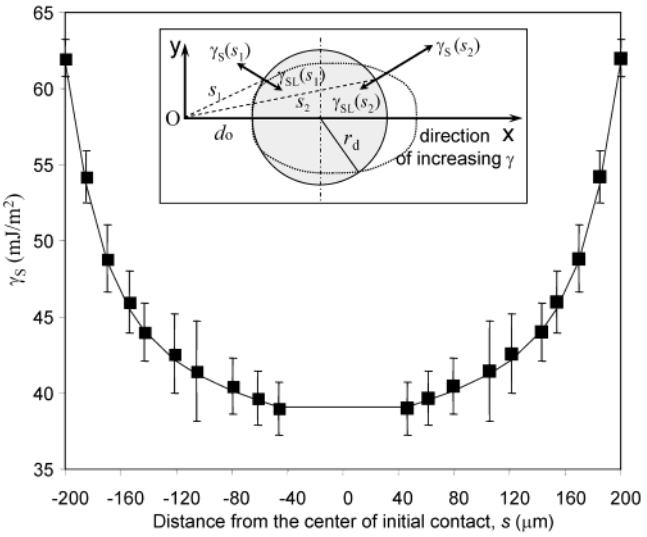

Figure 6. Experimentally estimated surface energies (■) for the gradient surface of Figure 5a are presented, and they are utilized to analyze the forces acting on the droplets. The surface energies were estimated based on the contact time of each contact-printed step. The correlation between the surface energy and the contact time was found to be $\gamma_S = 69t^{-0.15}$ for the larger-scaled contact-printed OTS surfaces. The distance from the center of the initial contact (O) was obtained from optical microscopy images taken during contact printing, and then the empirical relationship between γ_S and s could be obtained for this particular surface and used for further analysis. In the inset, the positional relationship of the droplet was sketched for the analysis.

Analysis of Droplet Movement on Gradient Surfaces. In its simplest form, the driving force (F_D) for a droplet moving on a surface can be expressed as[35]

$$F_D = L_2(\gamma_S - \gamma_{SL})_2 - L_1(\gamma_S - \gamma_{SL})_1 \qquad (1)$$

where L_1 and L_2 are the lengths of the three-phase contact lines that are perpendicular to the forces exerted from the surface (γ_S) and interfacial (γ_{SL}) energies at the two opposite edges (1 and 2) of the droplet. For an energy gradient surface, γ_S and γ_{SL} depend on the locations (s) and the geometry of the base perimeter of the droplet; therefore, it is more adequate to express F_D as

$$F_D = \int[\gamma_S(s_2) - \gamma_{SL}(s_2)]\,dL - \int[\gamma_S(s_1) - \gamma_{SL}(s_1)]\,dL \qquad (2)$$

where $\gamma(s_1)$ and $\gamma(s_2)$ are the energies at locations having respective distances of s_1 and s_2 away from the reference point, and dL is incremental length of the base perimeter of the three-phase contact line. For the gradient surface shown in Figure 5a, the positional-dependent energies were obtained and are shown in Figure 6. The energy values were obtained using the correlation of experimentally measured energy values versus the contact time on larger-scale OTS contact-printed surfaces and the known contact time for each contact position on the micrometer-scaled surface. The distance of each contact position was acquired using images captured from the videotape that recorded the entire contact-printing process for generating this particular gradient. For the four droplets 1 (~60 × 80 μm elliptical-shaped base, ~30 μm away from the edge), 2 (base diameter ~55 μm, ~30 μm away from the edge), 3 (base diameter ~70 μm, ~20 μm away from the edge), and 5 (base diameter ~100 μm, ~40 μm away from the edge) mentioned in the previous section that moved as a result of the energy gradient, the F_D values were estimated to be around 0.9, 0.5, 0.8, and 0.9 μN, respectively. These values are slightly smaller than but comparable to the values (1−10 μN) obtained experimentally by Suda and Yamada.[36] In their study, the droplet had a base diameter (D_d) of 2 mm and an energy gradient steepness ($\Delta\gamma/\Delta s$) of 2 N/m^2, while in our case, the droplet has a base diameter of 50−100 μm and an average gradient steepness of 100 N/m^2. Because $F_D \sim D_d^2(\Delta\gamma/\Delta s)$ for spherically capped droplets, to obtain the same driving force, a 1 order of magnitude reduction in the droplet size requires a 2 orders of magnitude increase in the gradient steepness.

Apart from the driving force, the total external forces (F_T) acting on the droplet include the force arisen from the contact-angle hysteresis (F_h), which plays a dominant role in resisting the movement of a droplet on a gradient surface.[32,35,37] This force, acting in the opposite direction as that of F_D, causes the pinning of the three-phase contact line. Roughly, the total external force acting on the droplet equals the difference between F_D and F_h. It can be estimated by integrating the unbalanced Young's force over the periphery of the droplet

$$F_T = F_D - F_h = \gamma_L\int[\cos\theta_a(s_2) - \cos\theta_r(s_1)]\,dy$$

$$F_h = F_D - \gamma_L\int[\cos\theta_a(s_2) - \cos\theta_r(s_1)]\,dy \qquad (3)$$

where $\theta_a(s_2)$ and $\theta_r(s_1)$ are the advancing and receding contact angles of the droplet formed on the surface at locations s_2 and s_1 away from O, respectively. Because the gradient surface in Figure 5a only had a size of 400 μm across, it was difficult to obtain the actual contact angles on its surface at different locations along the gradient. As a result, the empirical advancing and receding water contact angles (Figure 7) on such surfaces were obtained in a similar manner as the energy values. On the basis of Figure 7, at any particular distance away from O, the value of cos $\theta_r(s_1)$ or cos $\theta_a(s_2)$ was roughly deduced, and the value was then applied to estimate F_h. For all seven water droplets 1−7 in Figure 5a, the F_h values computed ranged from 1 to 2 μN. These values were comparable to and even slightly higher than the F_D values estimated (F_D values were 0.2, 0.2, and 0.4 μN for droplets 4, 6, and 7, respectively). The slightly higher estimated F_h values could be the result of excluding some details in our analysis. These details include, but are not limited to, the distortion of the water droplet from its modeled spherical cap and the possible differentiation between the actual surface-energy and contact-angle hysteresis at a particular location on the surface and those estimated from the empirical relationships. The energy gradient causes the droplet to elongate along the gradient direction, resulting in an elliptical base instead of the circular one, thus increasing the energy difference (or driving force) acting on the droplet. When we considered a 25% increase in the longitude of the droplet (the dotted outline of the droplet in Figure 6) while maintaining the base area covered by the droplet, a 50−70% and a 25−30% increase in F_D and F_h, respectively, resulted. Obviously, the increase in the driving force is more dramatic than that of the hysteresis force when the droplet distortion due to the energy gradient is considered. Furthermore, a 10% variation of the contact-angle value would lead to an ~25% difference in the value

(35) Brochard, F. *Langmuir* **1989**, *5*, 432−438.
(36) Suda, H.; Yamada, S. *Langmuir* **2003**, *19*, 529−531.
(37) Daniel, S.; Chaudhury, M. K. *Langmuir* **2002**, *18*, 3404−3407.

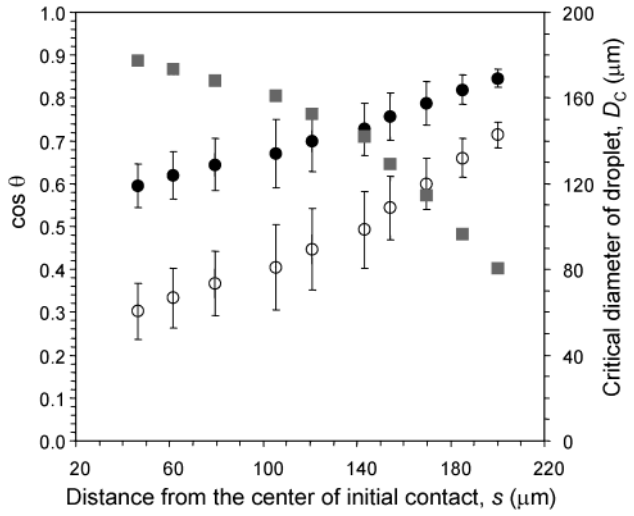

Figure 7. Estimated advancing (○) and receding (●) contact angles of water on the particular gradient surface shown in Figure 5a. The hysteresis appeared to decrease from the center (low-energy region) toward the edge (high-energy region) of the gradient. The diameter (D_c) of the critical-sized droplet (■) was also summarized, and the trend indicated that droplets could be moved relatively easier when they were located closer to the edge of the gradient. For this particular gradient surface, the smallest droplet that could be moved based on our analysis, without considering the possible distortion of the droplet, was around 80 μm in base diameter, which is slightly larger than but comparable to the actual size of droplet moved.

of F_h. When these details are included, our analysis adeptly explains the movement of the droplets observed experimentally.

Another resistance that hinders the droplet movement is the viscous force within the droplet, which can be estimated as[35−37]

$$F_v \approx 1.5\pi\eta D_d v \ln(X_{max}/X_{min}) \quad (4)$$

where η is the viscosity of water, D_d is the base diameter of the droplet, v is the velocity traveled by the droplet, and X_{max} and X_{min} are two cutoff lengths associated with the droplet. Normally, X_{max} can be taken as the base diameter of the droplet, and X_{min} is the molecular dimension and generally has a value close to 1 Å. For the water droplets that we studied in detail (Figure 5a), the viscous forces were only around 0.005−0.01 μN, much less than the hysteresis force. This agrees well with other studies; mainly, for smaller droplets, the contact-angle hysteresis becomes more predominant in resisting fluid flow on a gradient surface.

The critical droplet size as well as the velocity and the distance a droplet travels on a gradient surface strongly depend on the gradient steepness[11,16] and the droplet location. Figure 7 also shows the critical droplet size that can be moved by the energy gradient on the particular gradient surface of Figure 5a. The critical diameter of the droplet (D_c) is estimated by setting $F_T = 0$ and follows the analyses of Brochard[35] and Daniel and Chaudhury[37] by expressing $\cos\theta_a(s_2)$ and $\cos\theta_r(s_1)$ in terms of the values $\cos\theta_{a0}$ and $\cos\theta_{r0}$ at the central line of the droplet, and k is the slope of the linear fit of $(\cos\theta_a + \cos\theta_r)/2$ versus s:

$$D_c = 4(\cos\theta_{r0} - \cos\theta_{a0})/k\pi \quad (5)$$

For this particular gradient surface, the energy gradient steepness (Figure 6) increases gradually with the distance, from 20 to 100 N/m^2, within 140 μm away from O. From 140 to 200 μm away from O, the steepness increases dramatically from ∼100 to ∼700 N/m^2. The steepness of our gradient surfaces is 1−3 orders of magnitude higher than those reported by others.[16,36,37] On this gradient surface, a water droplet with a base diameter down to 80 μm can be moved. On other gradient surfaces with different gradient steepnesses, the movement of a water droplet with a base diameter as small as 20 μm was also observed. Smaller droplets are relatively easier to move when they are located closer to the edge of the gradient. The velocity of the droplet moving on such gradient surfaces can be estimated by equating F_T to F_v. For the particular water droplets in our study, the velocity was estimated to be on the order of 10 μm/s to 10 mm/s and depended on the exact surface-energy and contact-angle hysteresis at any particular location on the surface. Although the exact values of surface energies and contact angles were difficult to obtain experimentally, the values estimated from the empirical relationships were able to reasonably elucidate the experimental observations of the water-droplet movement on the gradient surface.

Concluding Remarks

We have developed a quick, convenient, and inexpensive method for generating gradient surfaces with minimum waste generation. In particular, we adopted the contact printing of OTS technique and tuned the OTS surface coverage by varying the contact time during contact printing. The gradient can be achieved by gradually decreasing the contact time as the contact area increases during contact printing. The approach could be extended to other molecules that have a time-dependent reaction with the substrate and can be utilized for contact printing. Micrometer-scaled gradient surfaces with steep gradients can be accomplished using a micromanipulator with the appropriate controls. The geometry and size of the contact-printed area depend on the shape and radius of curvature of the stamp, which can be fabricated easily using silicone elastomers. The gradient steepness can be controlled by the combination of the contact increment and contact time during contact printing. Our approach successfully generated micrometer-scaled gradient surfaces with a gradient steepness as high as ∼1000 N/m^2, which was 1−3 orders of magnitude higher than those generated using diffusion-based techniques. Tiny water droplets with volumes of hundreds of picoliters can be transported by the energy gradient on our gradient surfaces. One limitation of our approach is the small gradient steepness in regions close to initial contact (as is shown in Figure 6), and in some cases, the initial contact could be quite large, thus hindering the movement of droplets deposited on or around the initial contact regions. This limitation could be minimized by utilizing stamps with less compliant and smaller radii of curvature.

In addition to the capability of generating micrometer-scaled gradient surfaces using the contact printing of OTS approach, the movement of pico/nanoliter droplets on such surfaces suggests the possibility of using our approach to perform microfluidics on a surface. Microfluidics on surfaces will eliminate the complications associated with fabricating microdevices by etching into substrates and assembling external driving forces for fluid flow. It will also reduce the time and wastes associated with etching substrates and prevent the contamination and loss of fluids on the walls of the microdevices. Quick drainage of tiny droplets from the micrometer-scaled gradient surfaces was also observed, indicating possible applications of such gradient surfaces for minimizing condensation problems in heating/cooling systems or enhancing their heat-

transfer efficiencies. Micrometer-sized gradient surfaces, when made in the scale comparable to the size of a single cell (tens to hundreds of micrometers), could also be used to demonstrate how the substrate surface energy affects the interactions of integral membrane proteins of an individual cell with the substrate. Furthermore, by using micrometer-scaled gradient surfaces and an instrument having a micrometer-scaled magnification, the precise effects of the surface energy on the material behavior can be continuously monitored and analyzed for the entire energy range under a fixed monitoring position.

Experimental Section

Materials and Equipment. *n*-OTS and perfluorodecyl-1*H*,1*H*,2*H*,2*H*-trichlorosilane (FTS) were obtained from Gelest, Inc., and used without further purification. The organosilanes were sealed with Parafilm and stored in a vacuum desiccator prior to use. The PS (M_w = 65 000, pI = 1.03) was purchased from Polymer Source. The solvents used for the study were HPLC-grade hexane and toluene from J. T. Baker. Other chemicals used in this study included concentrated H_2SO_4 from Fisher and 30% H_2O_2 from VWR. The silicone elastomer, used for fabricating the stamps, was two-component (a base elastomer and a curing agent) Sylgard 184 from Dow Corning Corp. The substrates used were 4 in. test silicon wafers of P (100) purchased from Silicon Quest International. The micromanipulator was model 3926M ($x-y$ axis) from Parker Automation with in-house modifications. The cleaning equipment included a UV/ozone cleaner (model 42) from Jelight and an ultrasonic cleaner (model 50HT) from VWR. The characterization equipment was a contact-angle goniometer equipped with a charge-coupled device (CCD) video camera (model 100-00 from Rame-Hart, Inc.), optical microscopes (IX 70, Olympus and Infini Tube, Edmund Scientific) equipped with CCD video cameras, a scanning probe microscope (MI 2000 from Molecular Imaging), and an ellipsometer (model 439 from Rudolph Instruments, Inc.).

Fabrication of Elastomeric Stamps with Different Geometries. Sylgard 184 base elastomer and a curing agent were mixed according to the prescribed recipe. The mixture was then poured into a mold or onto a master to achieve the desired geometry. Stamps with three different geometries, hemispherical, hemicylindrical, and quartercylindrical, were generated. For the large hemispherical (radius of curvature, $R \sim 7$ mm) and hemicylindrical ($R \sim 7$ mm) stamps, an FTS-treated glass test tube with a round bottom was used as the mold. The smaller ($R \sim 1.5$ mm) hemispherical stamps were generated by dispensing small drops of the degassed silicone mixture onto a FTS-treated silicon wafer. The smaller hemicylindrical stamps were also generated by dispensing the degassed silicone mixture onto a narrow (width < 3 mm) strip of a FTS-treated silicon wafer. The quartercylindrical stamps were the hemicylindrical stamps cut into halves with a sharp blade. After the mixture was cured at room temperature for 48 h, the elastomeric stamps were peeled away from the molds or masters. All the fabricated stamps were extracted inside a Soxhlet extractor with toluene for 2 h to remove the un-cross-linked polymer chains.

Contact Printing of OTS with Different Contact Times. A cotton swab was dipped into a 2 mM solution of OTS in HPLC-grade hexane, and the solution was transferred from the cotton swab to the surface of the stamp. The inked stamp was dried with a stream of N_2. The stamp was then brought into contact with a cleaned and oxidized silicon wafer for a particular duration (1, 10, 20, 30, 60, 90, or 120 s) under slight finger pressure. For each sample, a new stamp was used with a freshly applied OTS solution. Each stamped silicon wafer was stored in a glass Petri dish at room temperature for 1 h to provide sufficient time for the OTS molecules to react with the silicon wafer. Then, it was sonicated in toluene for 2 min to remove the unreacted molecules. The OTS-modified substrates were then dried with N_2 gas. The same procedure was followed for each sample. The samples were characterized using contact-angle measurements, contact mechanics (JKR), ellipsometry, and SPM.

Generation and Characterization of Gradient Surfaces. For millimeter- or centimeter-scale gradients, the stamp was brought down, under slight finger pressure, into contact with a cleaned and oxidized silicon wafer to have an initial minimum contact area, and then the area of contact was increased gradually or stepwise by applying more pressure. For micrometer- or millimeter-scale gradients, the stamp was secured onto a cantilever attached to a micromanipulator. It was brought down into contact with the silicon wafer while the contact area was being monitored under an optical microscope video system. The increase of the contact area was controlled, either continuously or in a stepwise manner, using the micromanipulator. The entire contact-printing process was videotaped. The treatment of the stamped samples followed the same procedures as the contact-printed samples with different contact times. To verify and visualize the formation of the gradient surfaces, the dewetting of polymer thin films and water-droplet movement on the surface were performed. For the dewetting study, a PS thin film with a thickness of 800 Å placed on the gradient surface was annealed at 160 °C under ambient conditions. The annealing ceased when discernible dewetting hole formation was observed using the optical microscope video system. For the water-droplet movement study, the movement of water droplets, formed from a mist generated using an ultrasonic humidifier (HM-480, Holmes), was videotaped in real time using the optical microscope video system. Later, some images were captured while the tape was played. The droplet size, the distance traveled, and the velocity of the droplet were then measured. For a comparison study, experiments with PS thin film dewetting and water-droplet movement were performed on samples contact-printed with a uniform OTS coverage and having similar area sizes as their gradient counterparts.

Acknowledgment. We are grateful for financial support from the Start-Up Fund from the College of Engineering and the Department of Chemical Engineering at The University of Akron. Additional financial support from the Office of Research Services and Sponsored Program (UA FRG 1570) at The University of Akron is also appreciated. We thank Drs. Teresa Cutright and Rex D. Ramsier for valuable comments and suggestions. We also thank Mr. Frank S. Pelc for modifying the micromanipulator.

LA035027L